Structural phase transitions of sodium nitride at high pressure

G. V. Vajenine,[1,2,*] X. Wang,[1] I. Efthimiopoulos,[1] S. Karmakar,[1] K. Syassen,[1] and M. Hanfland[3]
[1]*Max-Planck-Institut für Festkörperforschung, Heisenbergstrasse 1, D-70569 Stuttgart, Germany*
[2]*Institut für Anorganische Chemie, Universität Stuttgart, Pfaffenwaldring 55, D-70569 Stuttgart, Germany*
[3]*European Synchrotron Radiation Facility, BP 220, F-38043 Grenoble, France*
(Received 22 December 2008; revised manuscript received 17 March 2009; published 8 June 2009)

The structural evolution of recently characterized sodium nitride Na_3N as a function of pressure was investigated at room temperature by the angle-dispersive powder x-ray diffraction in a diamond-anvil cell up to 36 GPa. The rather open cubic anti-ReO_3-type structure stable at ambient pressure is followed by a series of four high-pressure modifications. Along the route, the coordination number for the nitride anion increases from 6 in Na_3N-I to 8 in hexagonal Li_3N-type Na_3N-II, 9 in orthorhombic anti-YF_3-type Na_3N-III, 11 in hexagonal Cu_3P-type Na_3N-IV, and finally 14 in cubic Li_3Bi-type Na_3N-V structures. The experimental data are compared to the results of total-energy calculations and are discussed with regard to the structural details of the five phases and their equations of state.

DOI: 10.1103/PhysRevB.79.224107 PACS number(s): 62.50.−p, 61.50.Ks, 71.15.Nc

I. INTRODUCTION

Alkali-metal halides are textbook examples of stable ionic compounds between electropositive metals and electronegative nonmetals, featuring a nearly complete charge transfer of valence electrons according to the closed-shell configurations A^+X^- (A=Li-Cs, X=F-I). Similarly, all alkali-metal chalcogenides $A_2^+Q^{2-}$ (Q=O-Te) and most pnictides $A_3^+Pn^{3-}$ (Pn=P-Bi) are stable compounds; these have been characterized in detail as well. In contrast, labile nitrides of the heavier alkalis Na to Cs have been elusive until recently, with only lithium forming a stable binary nitride Li_3N.[1]

The first structural characterization of sodium nitride was carried out based on x-ray powder-diffraction data collected on films of Na_3N formed by depositing atomized elements on a cooled substrate.[2] Films of potassium nitride could be obtained in a similar way.[3] Recently, a practical route to produce larger amounts of sodium nitride was developed.[4] It is based on the reaction between a liquid Na-K alloy and plasma-activated nitrogen at room temperature. The initially proposed cubic anti-ReO_3-type ($Pm\bar{3}m, Z=1$) structure was confirmed for Na_3N based on x-ray diffraction data collected on powder and single crystals, and accessibility of the nitride on a laboratory scale allowed for further investigations of this unusual compound.[5]

In contrast to thermodynamically stable and colorless NaF and Na_2O, dark-blue semiconducting Na_3N is metastable with respect to the decomposition into elements at ambient pressure and temperature. It decomposes exothermally at around 100 °C. The thermal instability of sodium nitride can be qualitatively rationalized in the ionic limit. The coordination of the N^{3-} anion by only six singly charged and relatively large Na^+ cations leads to an insufficient electrostatic stabilization. The same argument can be used to explain the fact that the valence-band N $2p$ states lie relatively high in energy, which results in a narrow band gap.[6]

Not less intriguing is the very open crystal structure of Na_3N, featuring rare twofold linear coordination of the sodium cations (Fig. 1, topmost structure). The lattice constant of cubic sodium nitride (4.73 Å) is significantly larger than that of isostructural ReO_3 (3.73 Å) (Ref. 7) and Cu_3N (3.81 Å).[8] The resulting open network of Na_3N possesses a low density of only 1.3 g/cm^3 and might even be able to host small atoms and molecules.

Such an open structure is prone to collapse under pressure, and structural transformations are likely. So, lithium nitride Li_3N, which also has a rather unique open crystal structure, is known to transform from the ambient-pressure α modification ($P6/mmm, Z=1$) to a more compact Li_3P-type β phase ($P6_3/mmc, Z=2$) at 0.6 GPa, followed by an even-denser cubic Li_3Bi-type ($Fm\bar{3}m, Z=4$) γ modification[9,10] above 40 GPa. A number of potential structural candidates for sodium nitride have already been identified theoretically using the Hartree-Fock method.[11,12] Two of them, the hexagonal α-Li_3N- and Li_3P-type phases, were suggested to be more stable than the experimentally observed open cubic anti-ReO_3-type structure even at ambient pressure.[2]

We report here the structural phase transitions of Na_3N at high pressure in the range up to 36 GPa. By using the angle-dispersive synchrotron x-ray diffraction in combination with diamond-anvil cell techniques, four high-pressure modifications have been identified. The experimental observations are compared to the results of total-energy calculations for the identified phases.

II. EXPERIMENTS AND CALCULATIONS

Polycrystalline sodium nitride was prepared from a liquid Na-K alloy and plasma-activated nitrogen as described elsewhere.[4] For the synchrotron x-ray-diffraction measurements, the sample was ground to a fine powder and a small amount of it was transferred into the gasket of a diamond-anvil cell (DAC) with all handling carried out under inert argon atmosphere. No pressure medium was added during loading in order to avoid possible chemical reactions. Angle-dispersive powder x-ray-diffraction patterns (wavelength $\lambda = 0.412\,8$ Å) were measured at the beamline ID9 of the European Synchrotron Radiation Facility, Grenoble, using image-plate detection. The images (slightly spotty due to crystallite size effects) were integrated using the program

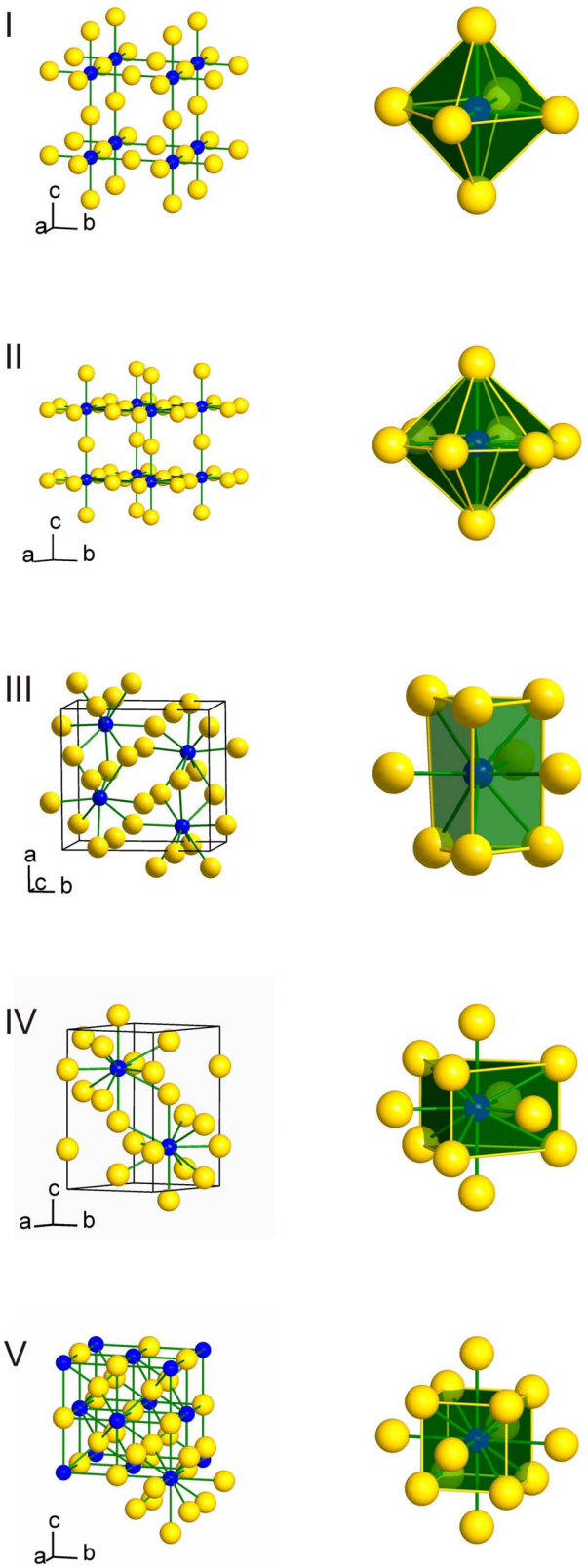

FIG. 1. (Color online) Crystal structures of phases I to V of Na_3N (left column) with the corresponding coordination polyhedra (right column) of sodium atoms (large, yellow spheres) around the nitrogen atoms (small, blue spheres). For the sake of clarity, the phase Na_3N-IV is represented by an undistorted Li_3P-type structure (see text for details).

FIT2D to yield intensity versus 2θ diagrams.[13] The relative intensities corresponding to the diffraction peaks of Na metal and Na_3N varied throughout the measurement series due to the inhomogeneous distribution of these phases in the sample. However, no sign of Na_3N decomposition was observed. To improve powder averaging, the DAC was oscillated by $\pm 3°$. The ruby-luminescence method was used for pressure measurement using the calibration of Mao *et al.*[14] Rietveld refinements of the powder-diffraction data were performed using the GSAS program.[15] Anisotropic peak broadening, especially relevant for the highest-pressure phase, was modeled by the microstrain broadening function of Stephens.[16] Atomic-temperature displacement factors were fixed at $U_{iso}=0.025$ Å^2 in most cases. The obtained R_p and R_{wp} values ranged from 7% to 12% and from 9% to 16%, respectively.

Total-energy calculations for different modifications of Na_3N were carried out by starting with the structural parameters derived from the diffraction data. The respective energy versus volume relations $E(V)$ were obtained by the full structural optimization at fixed volumes including variation in axial ratios and internal atomic parameters where appropriate. All calculations were carried out in the framework of the density-functional theory (DFT) using the full-potential augmented plane wave APW+lo method implemented in the WIEN2K package (version 06) (Ref. 17) with the Perdew-Burke-Ernzerhof generalized gradient approximation exchange-correlation potential.[18] The standard settings such as radii of the atomic spheres (R_{mt}) of 2.0 a.u. for all atoms and the cutoff condition $R_{mt} \times k_{max}=7$ for plane waves were employed. The size of the k-point mesh for the integration in the irreducible wedges of the respective Brillouin zones was chosen to achieve sufficient total-energy convergence for each structure. Due to the well-known underestimation of the fundamental band gap within DFT (see, e.g., Ref. 19), the computed band structures of most Na_3N modifications feature an overlap of conduction and valence bands by up to 0.6 eV. This artifact has been analyzed in detail for the ambient-pressure phase[6] and does not appear to significantly affect the results of total-energy calculations in this work.

III. RESULTS AND DISCUSSION

Two series of diffraction measurements were carried out. In a first exploratory run up to 30 GPa, the stability ranges of high-pressure modifications were identified and nearly complete reversibility was confirmed by observing, upon decompression, the diffraction patterns of all Na_3N modifications except that for Na_3N-III. In the second compression run, a more complete set of diffraction data up to 36 GPa was collected (see Fig. 2).

The ambient-pressure anti-ReO_3-type modification Na_3N-I was found to undergo four phase transformations under pressure. At 1.1 GPa, it transforms to the hexagonal Na_3N-II phase which is isostructural to α-Li_3N. Upon further pressure increase, two new modifications denoted Na_3N-III and Na_3N-IV appear simultaneously at 3.4 GPa. The phase Na_3N-III is orthorhombic and of the anti-YF_3 structure type; it is observed only up to 5.2 GPa. The phase Na_3N-IV is

hexagonal; it is structurally related to Li_3P and Cu_3P-type Na_3As. This fourth modification is followed by the cubic Li_3Bi-type Na_3N-V phase above 22.2 GPa, the last high-pressure modification observed up to the highest pressure of 36 GPa employed in this investigation.

We comment briefly on the refinements. Usually, the as-prepared samples are contaminated by not more than 10% metallic sodium. After loading into the DAC, the lowest-pressure Na_3N-I phase was found to contain a small amount (5%) of sodium oxide in addition to the impurity of metallic sodium. This is perhaps due to a surface contamination of the powderized samples before loading into a DAC. Both impurity phases retained their respective cubic structures throughout the entire pressure range covered in this study. The impurity phases were taken into account in the Rietveld refinements of high-pressure diffraction data.

Representative results of Rietveld refinements at different pressures and covering all observed phases of Na_3N are shown in Fig. 3. The related crystallographic details, i.e., unit-cell parameters, atomic-position parameters, and N-Na bond lengths, are summarized in Tables I–III. It should be noted that the listed standard deviations for refined parameters only take into account the statistics and are not considered to represent realistic errors.

The first structural transformation can be formally viewed as a folding of a square sublattice of Na_3N-I in the *ab* plane to a hexagonal one. The one-dimensional chains of alternating sodium and nitrogen atoms are preserved along the *c* axis in α-Li_3N-type Na_3N-II with space group $P6/mmm$ (Fig. 1). As a consequence, the position of the first (001) diffraction maximum at $2\theta \sim 5°$ is also preserved in this transition (Fig. 2). The coordination number of the nitrogen atom increases from 6 in the octahedron (Na_3N-I) to 8 in the hexagonal bipyramid (Na_3N-II). The sodium atoms in the *ab* plane increase their coordination number from two to three, while the remaining Na atoms stay linearly coordinated. The α-Li_3N-type structural model appears to be suitable for Na_3N-II based on the Rietveld analysis of the observed powder-diffraction patterns, especially when this phase is observed for the first time together with Na_3N-I at 1.1 GPa. However, some weak reflections, e.g., between 8° and 10° in patterns collected at higher pressures (cf. Fig. 3) could not yet be assigned (see also the discussion of Na_3N-III below). Although test calculations indicate that a displacement of the three-coordinate sodium atoms out of the *ab* plane does not cost much energy, no indication for such a structural distortion was found during the structural refinement; a related anti-α-UO_3-type[20] structure with puckered hexagonal Na_2N layers (also a structural candidate suggested for nitrides of heavier alkali metals[11]), when used as a starting point in a Rietveld refinement, was found to relax to the more symmetrical α-Li_3N-type structure in which these layers are flat.

The next high-pressure modification Na_3N-III was observed only in the range between 3.4 and 5.2 GPa. It was always accompanied by the Na_3N-IV phase and the maximum fraction of Na_3N-III was about 60%. Orthorhombic Na_3N-III is an antitype of the YF_3 structure[21] with space group *Pnma*; it contains nitrogen atoms surrounded by a triply capped trigonal prism of sodium atoms, a polyhedron frequently observed in halides of rare-earth metals (Fig. 1).

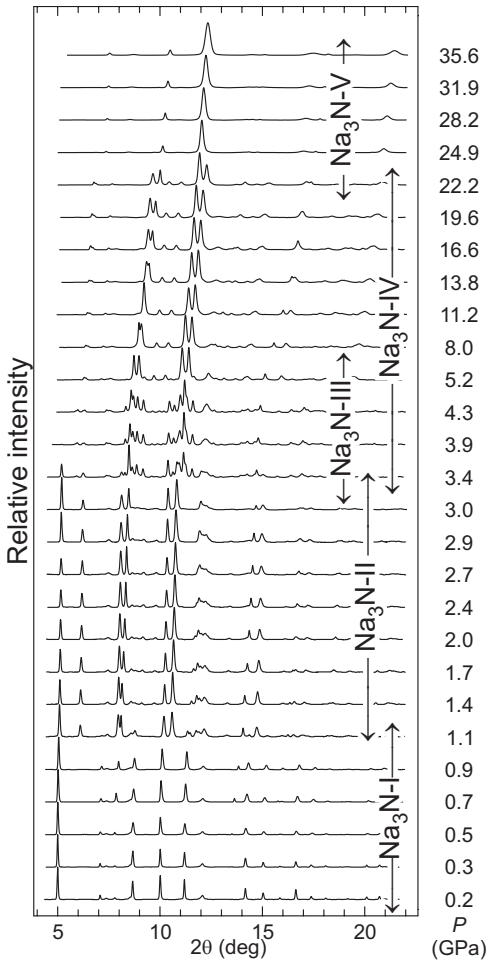

FIG. 2. A series of x-ray diffraction diagrams for Na_3N for increasing pressure collected using synchrotron radiation of 0.412 8 Å wavelength. Stability ranges for different structural modifications are indicated by arrows.

All sodium atoms are three coordinated by a nearly planar arrangement of the neighboring nitrogen atoms. This lower-symmetry structure type allows for some flexibility; the capping atoms can be moved further away from the central atom of the polyhedron without change in the space group by merely changing the atomic parameters and axial ratios resulting in the related Fe_3C structure type[22] with 6+2=8 coordination.

Both Rietveld analysis of the diffraction data and structural optimization indicate that nitrogen atoms in Na_3N-III are indeed nine coordinated according to the anti-YF_3-type structure with only a moderate difference between the shortest (2.45 Å) and the longest (2.75 Å) N-Na contacts (Table III). However, it is not clear yet whether the more open Fe_3C-type modification, featuring eight-coordinate nitrogen, is responsible for the above-mentioned additional weak-diffraction maxima that are seen in the pressure range where Na_3N-II is observed. If this were the case, an intermediate formation of the Fe_3C-type phase could lead to the anti-YF_3-type Na_3N-III modification in a space-group-preserving transformation. Such a transition path possibly explains why Na_3N-III is observed experimentally despite the fact that it appears metastable with respect to Na_3N-IV

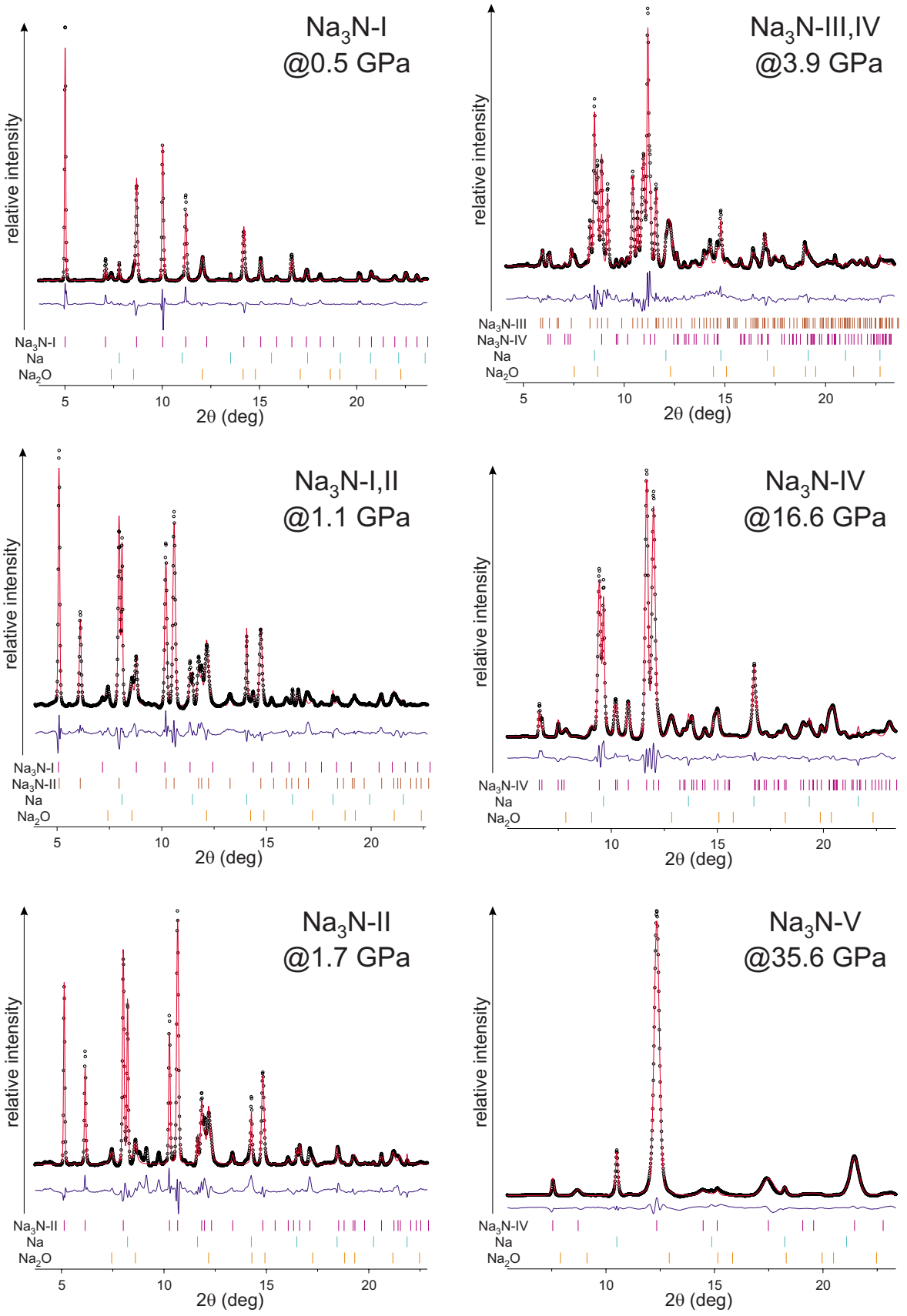

FIG. 3. (Color online) Representative Rietveld refinements of x-ray diffraction data for Na_3N phases I to V collected at different pressures (wavelength $\lambda = 0.412\,8$ Å). Open circles show the experimental patterns while lines represent the calculated and difference curves, respectively. Positions of the diffraction maxima for the respective phases and impurities are indicated with vertical tics.

TABLE I. Structural data for the modifications I to V of Na_3N based on Rietveld refinements of x-ray diffraction data presented in Fig. 3.

Phase	P (GPa)	Structure type	Space group Z	Lattice parameter (Å)	V (Å^3)	V/Z (Å^3)
I	0.0	anti-ReO_3	$Pm\bar{3}m$, 1	a=4.73301(6)	106.026(4)	106.026(4)[a]
I	0.5	anti-ReO_3	$Pm\bar{3}m$, 1	a=4.7244(1)	105.449(5)	105.449(5)
II	1.7	Li_3N	$P6/mmm$, 1	a=4.4414(3) c=4.6133(4)	78.81(1)	78.81(1)
III	3.9	anti-YF_3	$Pnma$, 4	a=7.090(1) b=7.518(1) c=4.794(1)	255.50(7)	63.88(2)
IV	16.6	Cu_3P	$P6_3cm$, 6	a=7.0356(4) c=7.1661(6)	307.20(3)	51.199(5)
V	35.6	Li_3Bi	$Fm\bar{3}m$, 4	a=5.4322(3)	160.29(1)	40.074(3)

[a]Reference 4.

according to our theoretical results (see below). In addition, this may also explain the fact that Na_3N-III, possibly kinetically accessible only in a compression run through the Fe_3C-type precursor, has not been observed during decompression, in contrast to the other phases of Na_3N. This point is left to be clarified in further investigations.

Most of the diffraction maxima of Na_3N-IV observed between 3.4 and 22.2 GPa can be described in a satisfactory manner by the hexagonal Li_3P structure type[23] which is also realized in β-Li_3N stable between 0.6 and 40 GPa. The coordination number of the nitrogen atoms is further increased to 11. The coordination polyhedron can be described as a fivefold-capped trigonal prism (Fig. 1). In this structure type, common to a number of alkali-metal pnictides, the nonmetal atoms form a hexagonal close-packed array, while two thirds of the metal atoms fill all tetrahedral voids. The remaining one third of the metal atoms lies within the hexagonal layers of the pnictogen atoms and have trigonal-planar environment. However, in the case of the alkali metals heavier than lithium, the formation of a $\sqrt{3}\times\sqrt{3}$ superstructure in the ab plane has been recognized, as in hexagonal Cu_3P-type[24] Na_3As.[25,26] This can be simplistically rationalized by an increased repulsion between larger alkali-metal atoms, which tend to move out of the high-symmetry positions of the Li_3P-type structure in order to minimize such repulsion, particularly between atom pairs occupying neighboring tetrahedral voids sharing a common face. This motion is however geometrically frustrated in the hexagonal parent structure and thus does not yield one clearly favored superstructure.

The Cu_3P structure type with the space group $P6_3cm$ and Z=6 is just one such possibility. It has been reported not only for other alkali-metal pnictides such as K_3Bi (Ref. 27) and Cs_3As (Ref. 28) but also in a number of intermetallic phases.[29–34] Another possibility with the same metric is the trigonal antitysonite-type structure (space group $P\bar{3}c1$, Z=6) typical for fluorides of rare-earth metals with large cations such as LaF_3.[35,36] That structure was also initially considered for Na_3As.[37] In the case of Na_3N-IV, the $\sqrt{3}a\times\sqrt{3}a$ superstructure is formed, as is clearly indicated by, for example, reflections between 10° and 12° (Fig. 3). However, it was not possible to discriminate between the Cu_3P- and anti-LaF_3-type structures in our study; both structural candidates could be used for satisfactory Rietveld refinement of the diffraction data and both structures provide a minimal stabilization of approximately 0.02 eV compared to the parent Li_3P-type structure after the geometry optimization. At this point we, however, favor the assignment as Cu_3P-type structure in analogy to other alkali-metal pnictides.

The similarity between the high-pressure structural chemistry of Na_3N and Li_3N is completed by the most-dense fifth modification of sodium nitride. Similar to γ-Li_3N, Na_3N-V crystallizes in the cubic Li_3Bi (Ref. 23) structure type with alkali-metal atoms occupying all octahedral and tetrahedral voids of a cubic close-packed arrangement of nitrogen atoms (Fig. 3). This also leads to the maximum coordination number of 14 for the nitrogen atoms. The nitrogen atoms are surrounded by mutually interpenetrating cubes and octahedra, merging to rhombic dodecahedra (Fig. 1).

Table III summarizes the N-Na bond lengths in the observed Na_3N modifications at selected pressures. If one follows the evolution of these values in detail, the well-known apparent pressure-bond-length paradox[38] becomes evident; each phase transition from a low- to a high-pressure modification is accompanied by a steplike increase in the average N-Na bond lengths which then shorten upon raising the pressure. The overall change in bond lengths over the five phases is small. The nearest-neighbor N-Na contacts in Na_3N-V are not much shorter than those in Na_3N-I. So, the large increase in density of Na_3N is achieved mainly by increasing the atomic coordination.

Figure 4 shows the experimental volume per formula unit as a function of pressure for all five modifications of Na_3N. The rather open ambient-pressure Na_3N-I phase undergoes a large overall volume change under pressure on the way to the most-dense modification Na_3N-V. At the highest pressure of 36 GPa, Na_3N is compressed to 38% of its ambient-pressure volume. The changes in coordination number at the phase transitions are reflected in the volume discontinuities. Related data are listed in Table IV. For comparison and where appropriate, the relative volume changes at phase transitions in Li_3N are also listed in order to illustrate the similarity to Na_3N.

TABLE II. Fractional atomic parameters for the Na_3N modifications I to V based on Rietveld refinements of the diffraction data presented in Fig. 3 (cf. Table I). The theoretical values for variable parameters in phases II and III corresponding to the respective experimentally observed unit-cell volumes are given in parentheses for comparison.

Atom	Position	x	y	z
		Na_3N-I at 0.5 GPa		
N	1*a*	0	0	0
Na	3*d*	$\frac{1}{2}$	0	0
		Na_3N-II at 1.7 GPa		
N	1*a*	0	0	0
Na1	1*b*	0	0	$\frac{1}{2}$
Na2	2*c*	$\frac{1}{3}$	$\frac{2}{3}$	0
		Na_3N-III at 3.9 GPa		
N	4*c*	0.376(2)	$\frac{1}{4}$	0.057(3)
		(0.3643)		(0.0592)
Na1	4*c*	0.026(1)	$\frac{1}{4}$	0.915(2)
		(0.0252)		(0.9185)
Na2	8*d*	0.162(1)	0.072(1)	0.384(1)
		(0.1597)	(0.0659)	(0.3888)
		Na_3N-IV at 16.6 GPa		
N	6*c*	0.357(3)	0	0.250(3)
		(0.3289)		(0.2544)
Na1	2*a*	0	0	0.289(2)
				(0.3093)
Na2	4*b*	$\frac{1}{3}$	$\frac{2}{3}$	0.228(2)
				(0.2270)
Na3	6*c*	0.298(1)	0	0.571(1)
		(0.2931)		(0.5841)
Na4	6*c*	0.362(1)	0	0.912(1)
		(0.3706)		(0.9264)
		Na_3N-V at 35.6 GPa		
N	4*a*	0	0	0
Na1	4*b*	$\frac{1}{2}$	$\frac{1}{2}$	$\frac{1}{2}$
Na2	8*c*	$\frac{1}{4}$	$\frac{1}{4}$	$\frac{1}{4}$

All volume-versus-pressure results were fitted by a third-order Birch equation of state (EOS).[39] For each phase i, the volume at the lowest pressure V_i was taken as the reference volume. In this way, we have avoided questionable back extrapolations to the hypothetical zero pressure. In all fits, the values of the pressure derivative of the bulk modulus were fixed at $B_i'=4$. The obtained values B_i of the bulk modulus (see Table V) increase in a systematic manner with increasing density of phase i.

The calculated total energies as a function of volume are shown in Fig. 5. Again, all results were fitted by the appropriate third-order Birch expression. The computed equations

TABLE III. N-Na bond lengths (Å) in the Na_3N modifications I to V based on Rietveld refinements of the diffraction data presented in Fig. 3 (see also Tables I and II). The multiplicities of symmetry equivalent nearest-neighbor contacts are given in reference to nitrogen atoms. The theoretically optimized bond lengths corresponding to the respective experimentally observed unit-cell volumes are given for comparison.

Phase	$d_{\text{N-Na}}^{\text{expt}}$	$d_{\text{N-Na}}^{\text{calc}}$	
Na_3N-I at 0.5 GPa	$6\times2.36220(7)$	6×2.362	$=a_I/2$
Na_3N-II at 1.7 GPa	$2\times2.3067(2)$	2×2.344	$=c_{II}/2$
	$6\times2.5642(2)$	6×2.544	$=a_{II}/\sqrt{3}$
Na_3N-III at 3.9 GPa	$2\times2.45(1)$	1×2.497	
	$1\times2.50(1)$	2×2.518	
	$2\times2.56(1)$	2×2.523	
	$1\times2.57(1)$	2×2.555	
	$2\times2.57(1)$	1×2.563	
	$1\times2.75(1)$	1×2.757	
Na_3N-IV at 16.6 GPa	$2\times2.27(1)$	1×2.347	
	$1\times2.29(2)$	1×2.369	
	$1\times2.34(2)$	2×2.369	
	$1\times2.42(2)$	1×2.376	
	$1\times2.53(2)$	1×2.447	
	$2\times2.66(2)$	2×2.515	
	$1\times2.75(2)$	2×2.764	
	$2\times2.78(1)$	1×2.927	
Na_3N-V at 35.6 GPa	$8\times2.3522(1)$	8×2.352	$=\sqrt{3}a_V/4$
	$6\times2.7161(1)$	6×2.716	$=a_V/2$

TABLE IV. Relative volume changes at first-order phase transformations of Na_3N. Experimental and calculated volume differences refer to the indicated pressure values. Where applicable, the results for the related transformations in Li_3N are given in parentheses.

		$\frac{V_i/Z_i - V_j/Z_j}{V_i/Z_i}$ (%)	
Phases $i\rightarrow j$	P (GPa)	Expt.	Calc.
I→II	1.1	20.9	22.1
II→III	3.4	14.6	
III→IV	3.4–5.2	4.3	
II→IV	3.4	18.3	18.2
($\alpha\rightarrow\beta$)	(0.6)[a]	(22.8)[a]	
IV→V	22.2	8.1	8.2
($\beta\rightarrow\gamma$)	(40)[b]	(8)[b]	(6.7)[b]

[a]Reference 9.
[b]Reference 10.

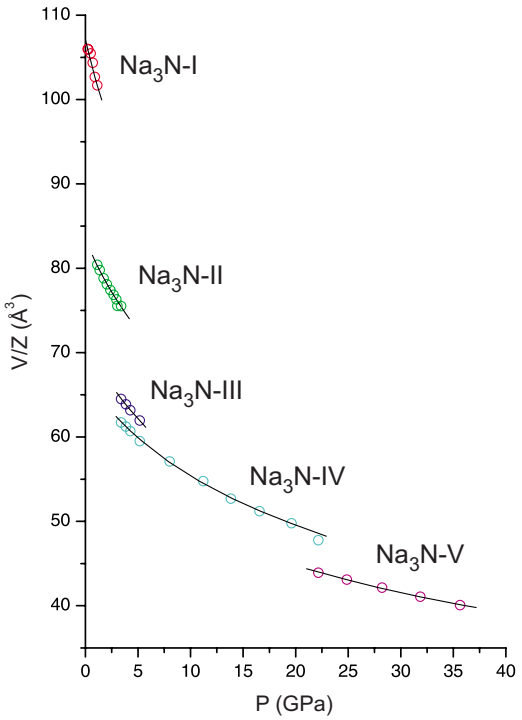

FIG. 4. (Color online) Experimental volume versus pressure data (open circles) for five modifications of Na_3N. Solid curves represent results of least-squares fits using the third-order Birch EOS. The parameter values are given in Table V.

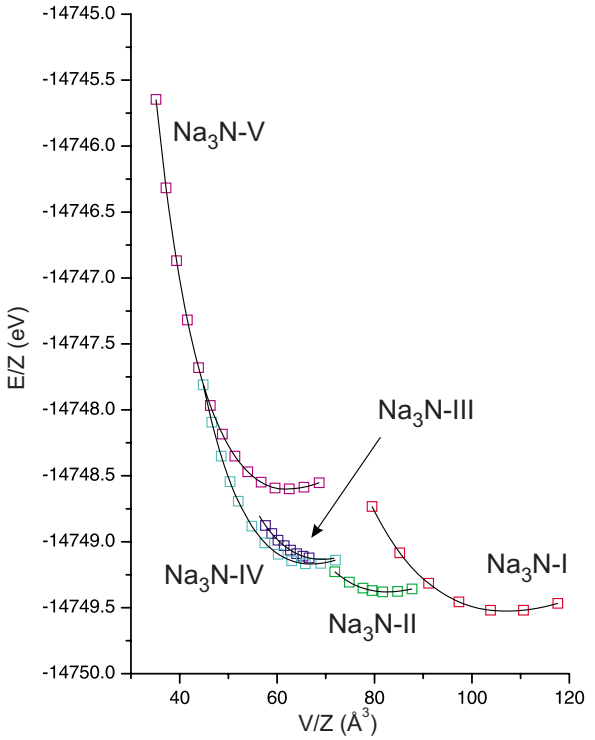

FIG. 5. (Color online) Calculated total energies of the Na_3N modifications I to V (open squares). Solid curves show fits with the third-order Birch EOS with parameters given in Table V.

of state for the five phases of sodium nitride agree quite well with the observed behavior. This applies to the volume differences between phases (see Table IV and the bulk-modulus values as well as stability ranges listed in Table V. Only Na_3N-III lies slightly higher in energy (by ~0.15 eV per formula unit) than expected based on the experimental findings. This is however consistent with the narrow pressure range in which the phase is observed and with the fact that it was not observed in pure form, possibly, due to the above-mentioned kinetic stabilization of this phase.

When the structure optimization of anti-YF_3-type Na_3N-III in *Pnma* with V/Z larger than 67 Å^3 was attempted, a substantial relaxation into a Fe_3C-type structure was observed. As a result, we cannot assign a calculated value of V_0 to the anti-YF_3-type phase and this is the reason for the missing value in Table V.

The calculated values of axial ratios of the noncubic phases of Na_3N were found to be in good agreement with the experimental data. For Na_3N-II, the calculated value of 1.064 for the c/a ratio is slightly larger than the observed value of 1.039. For Na_3N-II, the optimized c/a (0.678) and b/a (1.103) ratios also are somewhat larger than the observed values of 0.676 and 1.060, respectively. For Na_3N-IV, the optimized value of c/a is 1.023 compared to 1.019 from the experiment. Small deviations in calculated axial ratios are not uncommon in DFT-based structure optimizations of noncubic phases.

The calculated values of free-atom position parameters of phases II and III are given in Table II and the corresponding calculated bond lengths can be found in Table III. There is no major discrepancy between refined and calculated values.

TABLE V. Stability ranges and bulk moduli (all in GPa) for the Na_3N modifications I to V based on experimental data in comparison to the results of total-energy calculations fitted with third-order Birch EOS. The calculated equilibrium volumes $V^{calc}(0)/Z$ are given in Å^3.

	Expt.		Calc.			
Na_3N phase	$P^{expt}_{min}-P^{expt}_{max}$	$B^{expt}(P^{expt}_{min})$	$P^{calc}_{min}-P^{calc}_{max}$	$V^{calc}(0)/Z$	$B^{calc}(0)$	$B^{calc}(P^{expt}_{min})$ [a]
I	0–1.1	20.4(2)	0–1.0	107.07(8)	21.9(2)	21.9
II	1.1–3.4	31.9(9)	1.0–2.3	82.70(4)	27.4(2)	32.0
III	3.4–5.2	40(2)			31.7(2)	45.3
IV	3.4–22.2	49(1)	2.3–25.0	66.8(1)	31.4(5)	45.0
V	above 22.2	121(6)	above 25.0	61.6(3)	33.4(7)	122.1

[a]Estimated according to $B^{calc}(P^{exp}_{min})=B^{calc}(0)+B'P^{expt}_{min}$ with $B'=4$.

This enhances the confidence in the refined structural parameters.

As noted, the calculated band structures of the Na_3N modifications I to IV feature an overlap of conduction and valence bands by up to 0.6 eV. However, the calculated negative band gaps are small compared to the typical band-gap error of DFT calculations. So, the calculations do not necessarily imply the metallic character of these Na_3N modifications. Actually, in Na_3N-V a band gap opens up in the calculations, similar to the initial band-gap increase found for Li_3N with increasing pressure.[10] A further discussion of electronic properties of Na_3N under pressure is not within the scope of this work and would also not be very meaningful at this point because of the lack of experimental data.

In summary, the observed evolution of the sodium-nitride crystal structure under pressure represents a nice example for the potential richness of pressure-induced phase transformations in ionic AB_3 compounds. At pressures up to 36 GPa, four high-pressure modifications have been identified and three of the phase transitions are reversible. In the direction of increasing pressure, the sequence of phases can be easily rationalized by the steady increase in the coordination number of the nitrogen atoms from 6 over 8, 9, and 11 to finally 14, along with an increase in sodium coordination numbers as well. Since the increasing coordination number together with nearly constant average N-Na distances improves the electrostatic stabilization of the nitride anion, the thermodynamic stability of Na_3N with respect to the elements should increase with increasing pressure. In addition, since one of the decomposition products (nitrogen) is a gas under ambient conditions, the stabilizing effect of high pressure is enhanced even further. As a result, sodium nitride might become thermodynamically stable under high pressure. Moreover, the high-pressure route might be also a promising way to stabilize even more labile nitrides of heavier alkali metals K to Cs, perhaps with structures such as those observed in this study.

ACKNOWLEDGMENTS

G.V.V. would like to thank A. Simon for the support in this project as well as H.-J. Deiseroth, Th. Schleid, and J. C. Schön for helpful comments.

*Corresponding author; g.vajenine@fkf.mpg.de

[1] E. Zintl and G. Brauer, Z. Elektrochem. Angew. Phys. Chem. **41**, 102 (1935).
[2] D. Fischer and M. Jansen, Angew. Chem., Int. Ed. **41**, 1755 (2002).
[3] D. Fischer, Z. Cancarevic, J. C. Schön, and M. Jansen, Z. Anorg. Allg. Chem. **630**, 156 (2004).
[4] G. V. Vajenine, Inorg. Chem. **46**, 5146 (2007).
[5] G. V. Vajenine, Solid State Sci. **10**, 450 (2008).
[6] B. Baumeier, P. Kruger, J. Pollmann, and G. V. Vajenine, Phys. Rev. B **78**, 125111 (2008).
[7] K. Meisel, Z. Anorg. Allg. Chem. **207**, 121 (1932).
[8] R. Juza and H. Hahn, Z. Anorg. Allg. Chem. **239**, 282 (1938).
[9] H. J. Beister, S. Haag, R. Kniep, K. S. Ner, and K. Syassen, Angew. Chem., Int. Ed. Engl. **27**, 1101 (1988).
[10] A. Lazicki, B. Maddox, W. J. Evans, C.-S. Yoo, A. K. McMahan, W. E. Pickett, R. T. Scalettar, M. Y. Hu, and P. Chow, Phys. Rev. Lett. **95**, 165503 (2005).
[11] M. Jansen and J. C. Schön, Z. Anorg. Allg. Chem. **624**, 533 (1998).
[12] J. C. Schön, M. A. C. Wevers, and M. Jansen, J. Mater. Chem. **11**, 69 (2001).
[13] A. P. Hammersley, S. O. Svensson, M. Hanfland, A. N. Fitch, and D. Hausermann, High Press. Res. **14**, 235 (1996).
[14] H. K. Mao, J. Xu, and P. Bell, J. Geophys. Res. **91**, 4673 (1986).
[15] A. C. Larson and R. B. Von Dreele, General Structure Analysis System (GSAS), Los Alamos National Laboratory Report No. LAUR 86-748 (2004).
[16] P. Stephens, J. Appl. Crystallogr. **32**, 281 (1999).
[17] P. Blaha, K. Schwarz, G. K. H. Madsen, D. Kvasnicka, and J. Luitz, WIEN2K: an augmented plane wave+local orbitals program for calculating crystal properties (2006).
[18] J. P. Perdew, K. Burke, and M. Ernzerhof, Phys. Rev. Lett. **77**, 3865 (1996).
[19] J. P. Perdew and A. Zunger, Phys. Rev. B **23**, 5048 (1981).
[20] W. H. Zachariasen, Acta Crystallogr. **1**, 265 (1948).
[21] A. Zalkin and D. H. Templeton, J. Am. Chem. Soc. **75**, 2453 (1953).
[22] S. B. Hendricks, Z. Kristallogr. **74**, 534 (1930).
[23] G. Brauer and E. Zintl, Z. Phys. Chem. Abt. B **37**, 323 (1937).
[24] O. Olofsson, Acta Chem. Scand. **26**, 2777 (1972).
[25] P. Hafner and K.-J. Range, J. Alloys Compd. **216**, 7 (1994).
[26] K.-J. Range, R. Ehrl, and P. Hafner, J. Alloys Compd. **240**, 19 (1996).
[27] H. Kerber, H. J. Deiseroth, and R. Walther, Z. Kristallogr.- New Cryst. Struct. **213**, 473 (1998).
[28] H. Hirt and H. J. Deiseroth, Z. Kristallogr.- New Cryst. Struct. **218**, 6 (2003).
[29] K. M. Alasafi and K. Schubert, J. Less-Common Met. **51**, 225 (1977).
[30] K.-J. Range and P. Hafner, J. Alloys Compd. **183**, 430 (1992).
[31] K.-J. Range and P. Hafner, J. Alloys Compd. **191**, L5 (1993).
[32] V. Hlukhyy, R. D. Hoffmann, and R. Pöttgen, Intermetallics **12**, 383 (2004).
[33] V. Hlukhyy, U. C. Rodewald, R. D. Hoffmann, and R. Pöttgen, Z. Naturforsch., B: Chem. Sci. **59**, 251 (2004).
[34] J. P. A. Makongo, C. Kudla, Yu. Prots, R. Niewa, U. Burkhardt, and G. Kreiner, Z. Kristallogr.- New Cryst. Struct. **220**, 289 (2005).
[35] M. Mansmann, Z. Anorg. Allg. Chem. **331**, 98 (1964).
[36] M. Mansmann, Z. Kristallogr. **122**, 375 (1965).
[37] M. Mansmann, Z. Kristallogr. **122**, 399 (1965).
[38] A. Neuhaus, Chimia **18**, 93 (1964).
[39] F. Birch, J. Geophys. Res. **83**, 1257 (1978).